Viewpoint Selection for Fibrous Structures in a Pre-operative Context: Application to Cranial Nerves Surrounding Skull Base Tumors

Méghane Decroocq, Morgane Des Ligneris, Timothée Jacquesson, Carole Frindel

Viewpoint Selection for Fibrous Structures in a Pre-operative Context: Application to Cranial Nerves Surrounding Skull Base Tumors

Méghane Decroocq[1][0000−0002−8370−4067], Morgane Des Ligneris[1][0000−0003−1008−3009], Timothée Jacquesson[2][0000−0001−9985−3617], and Carole Frindel[0000−0003−4570−0994]1

[1] Univ Lyon, INSA-Lyon, Université Claude Bernard Lyon 1, UJM-Saint Etienne, CNRS, Inserm, CREATIS UMR 5220, U1206, Lyon, France
[2] Skull Base Multi-disciplinary Unit, Neurological Hospital Pierre Wertheimer, Hospices Civils de Lyon, 59 Bd Pinel, Lyon, France
carole.frindel@creatis.insa-lyon.fr

Abstract. In this work, we present a viewpoint selection method specifically designed for fibrous structures in a pre-operative context. A view quality metric based on entropy was developed, which integrates the typical requirements of surgery planning. We applied our approach in the case of cranial nerves surrounding skull base tumors. The relevance of the viewpoints selected by our method was assessed qualitatively by a neurosurgeon and quantitatively based on statistical tests. These viewpoints were proven to have a high informative content, and therefore to enable a good understanding and mental representation the 3D anatomical scene in a pre-operative context.

Keywords: viewpoint selection · entropy · fiber tractography · cranial nerves · skull base tumor · surgical planning

1 Introduction

Skull base tumor surgery remains a challenge since it requires complex surgical approaches reaching deep-seated tumors within a dense anatomical environment [11]. This environment includes cranial nerves, which are bundles of white matter fibers with sensorial or motor functions (e.g the optic nerve). The preservation of the cranial nerves functions is one of the main stakes of tumor resection surgery. In this context, a thorough visualization of the nerves surrounding or displaced by the tumor could be of help for intervention planning, as attested by recent studies [2, 5, 13].

Advances in dMRI have used the unequal movement of water molecules along axons to reconstruct the 3 dimensional trajectory of the white matter fibers through tractography. However, tractography involves a complex multistep processing pipeline and is still difficult to apply to small-scale structures such as cranial nerves [6]. As a result, tractography datasets might be hard to visualize due to excessive amount of streamlines that are running in very different

directions. Moreover, it moves away from the conventional radiological practice where datasets are visualized in 2 dimensions (2D). In this context, the selection of the viewpoints which best enhances the display of the important anatomical structures, here the tumor and nerves, as well as the whole scene, is valuable for surgery planning. It would reduce the complexity of the data, facilitate the understanding of the scene in 3 dimensions and guide the selection of the operative viewpoint.

To our knowledge, viewpoint selection for tractography fibers has never been investigated in the literature. This idea has been explored for other anatomical structures like organs, bones, vessels and tumors [9] [3], but the proposed methods, based on geometrical criteria such as minimum distance or occlusion between objects, can hardly be applied to scattered and complex structures like tractography. Besides, one of the purposes of this work is to propose a local metric to prioritize the fibers according to their anatomical relevance. Prioritization of the structures of interest for medical applications was not introduced in any of the previous works.

Shannon's entropy quantifies the information content in a dataset, and is commonly used in the computer vision field to find informative viewpoints on meshes [1]. Moreover, it was shown to be an interesting measure to filter and visualize velocity streamlines [4], which have a nature close to tractography fibers. In this paper, we propose to use the local entropy of fibers as a selection metric to select the best viewpoints on a 3 dimensional scene including a tumor and surrounding nerves.

In section 2, we give details on the acquisition of the medical images, the tractography pipeline employed and the anatomy of the cranial nerves of interest. In section 3 we describe the application of Shannon entropy to tractography fibers and the calculation of the viewpoint quality score. Our validation strategy is explained. Finally, in the section 4, the quality of the selected views is assessed both qualitatively and quantitatively, demonstrating the pertinence of the selection method.

2 Material

2.1 Cranial Nerves

The fibers of the white matter connects the different areas of the brain. Cranial nerves are organized bundles of white matter fibers with important sensorial or motor functions. Five cranial nerves or nerve groups located near the skull base were considered in this study: the optic nerve (Chiasma); the oculomotor nerve (III); the trigeminal nerve (V); the fascial and cochleo-vestibular nerves group (NF) and the mixed nerves groups (NM). Their mean diameter was estimated according to the known anatomy [7, 10, 16], and reported in Table 1.

2.2 Patients

Patient data (n=31) used in this work is based on the study carried out between December 2015 and December 2017 in [5] (IRB Number 2015-A01113-46). In-

Table 1. Estimated diameter of the studied nerves from the literature.

Nerve definition	Nerve abbreviation	Diameter (mm)
Optic	Chiasma	10
Oculomotor	III	5
Trigeminal	V	7
Facial and cochleo-vestibular	NF	3
Mixed	NM	2

clusion criteria were: skull base tumor ; at least two cranial nerves in contact with the tumor; legal capacity; consent provided after fair information; 3T MRI data with dMRI acquisition. Exclusion criteria were: MR contraindications.

2.3 MRI Acquisition

A set of MR sequences were acquired in order to reconstruct the anatomical structures of interest. T1 post contrast weighted sequence and T2 steady state sequence are high resolution images(0.23 x 0.23 x 0.34 mm), which were used as an anatomical reference. The segmentation of the tumors was made manually from the T1 sequence by a neurosurgeon. Diffusion images were acquired in order to compute the trajectories of fibers. It encodes the local diffusion of water molecules in 32 directions. This modality have a lower spatial resolution (1.75 x 1.75 x 2 mm). Distortions were corrected using the top-up and eddy tools of the FMRIB software library (FSL) software [12].

2.4 Tractography

Tractography is the method used to reconstruct the trajectory of the white matter fibers from the diffusion images. Figure 1 shows both the tractography reconstruction and a per-operative view for the oculomotor nerve. In this study, the tractography process was carried out from the acquired diffusion images using the Mrtrix3 software [14]. A brain mask was drawn to restrain the fiber reconstruction to the brain area. A spherical constrained deconvolution (6 spherical harmonic terms) was used to create a map of orientation distribution function (ODF) from the 32 directions of diffusion images. Cubic region-of-interest for the initialization of the tractography were designed by overlaying the ODF map on the T2-weighted MRI in order to identify the location of the cranial nerves with a great precision. A probabilistic tractography algorithm was used for the tracking of cranial nerves from the regions of interest [5]. The minimum fiber length required for the tracking was set to 10 mm and the number of fibers of each nerve to be reconstructed was set from 200 to 1000 according to the estimated nerve diameter. The output is a list of the spatial coordinates of the fibers.

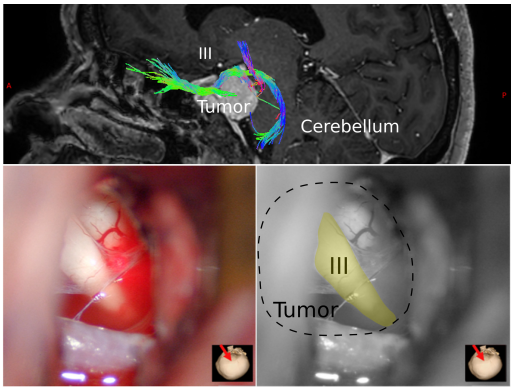

Fig. 1. Tractography fibers of the oculomotor nerve, superimposed on the T1 modality (top image). Post-operative view of the oculomotor nerve (bottom images). The position of the tumor before resection and the nerve trajectory are highlighted.

3 Methods

3.1 Entropy

Shannon's entropy is a measure commonly used in information theory, which quantifies the content of information in a dataset from its distribution. For a discrete random variable X with n classes, each class x_i having a probability $p(x_i)$ to appear, the entropy $e(X)$ is defined as:

$$e(X) = -\sum_{i=1...n} p(x_i) log_2(p(x_i)). \tag{1}$$

This measure can be easily applied to a vector field, by creating an orientation histogram of these vectors. With this orientation histogram, the probability of the vectors in the bin x_i, i. e. the vectors corresponding to a specific orientation, is calculated as:

$$p(x_i) = \frac{C(x_i)}{\sum_{i=1...n} C(x_i)}, \tag{2}$$

where $C(xi)$ is the number of vectors in bin x_i. Figure 2 illustrates this process in a two dimensional case for a case of orientation disorder (Fig. 2-a: low entropy) and of orientation coherence (Fig. 2-b: high entropy).

In a similar way, we can compute the entropy of the 3 dimensional vector field that encodes the local direction of the tractography fibers. In this way, entropy can be used to discriminate the fibers of homogeneous orientation, located in the core of the nerve, from the more chaotic fibers badly impacting the visual result. A low entropy indicates that the location contains structures of medical interest and need to be preserved and enhanced in the visualization. The conversion of the fibers into a vector field is described in Section 3.2.

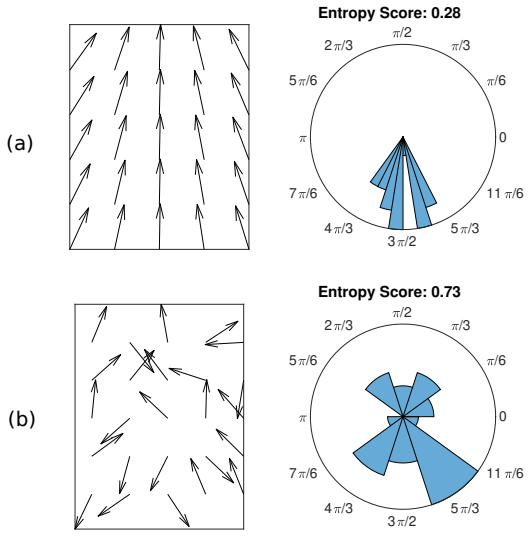

Fig. 2. Vector fields and their associated orientation histogram. The score given in the right column corresponds to the entropy value of the central vector calculated using a 3×3 neighborhood and 10 bins. The more the vector field is scattered the higher the entropy value.

3.2 Vector Field Reconstruction

To apply entropy to tractography data, we first need to obtain a vector field of local fiber orientations. This information could be extracted from the main eigenvector of the diffusion tensor estimated from the raw dMRI data. However, this method is very sensitive to noise, particularly because of the low resolution of the dMRI data (2 mm) compared to the diameter of the nerves (2-10 mm: cf Table 1). We therefore propose to reconstruct a vector field from the fibers themselves. These are indeed less sensitive to noise because they have undergone numerous post-treatments during the of tractography process. Considering that fibers are sampled more than 10 times finer than the dMRI voxel, the resolution of the final vector field can be drastically improved.

In this sense, the fibers are first transformed into a 3D image encoding the local fiber density information. Then, a map of the maximum intensity gradient direction of this image is calculated using a $3 \times 3 \times 3$ neighborhood according to the method in [15]. Since the gradient orientation is normal to the actual fiber orientation, the vectors are reoriented according to the average of the vector products of the central voxel and its neighbors in the $3 \times 3 \times 3$ neighborhood.

3.3 Entropy Map

In order to produce a three dimensional entropy map $E(x, y, z)$ that represents the local entropy value of the fibers, each voxel of coordinates (x, y, z) in the

vector field is associated to a small cubic neighbourhood $n \times n \times n$. Considering 3D vectors, an orientation histogram in the neighborhood of the considered voxel is computed. This is achieved in 3D by decomposing the unit sphere into patches of equal area [8], and using the cones connecting the patches to the center of the sphere as bins for the orientation histogram. Each vector in the neighborhood is assigned to the appropriate bin (i.e cone) and the computed entropy value is assigned to the corresponding voxel (x, y, z) in the 3D entropy map $E(x, y, z)$.

Based on Eq. (1) and (2), entropy map depends on two parameters; the number of bins n used in the histogram and the size of neighborhood considered to build the histogram. In our case, the parameters are chosen taking into account priors on the dMRI acquisition and the anatomy of the cranial nerves. The number of bins corresponds roughly to the number of diffusion directions used in dMRI acquisition and the neighborhood size is proportional to the diameter of the considered nerve, as given in Table 1.

The resolution of the computed vector field (see Section 3.2) also impacts the computed 3D entropy map. As shown by Figure 3, working at a better resolution makes it possible to use a neighborhood size for entropy computation smaller than the diameter of the nerve and hence to have a low entropy at the center of the nerve, as expected.

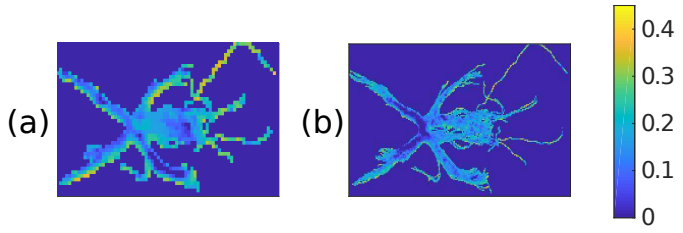

Fig. 3. Minimum entropy projections along the axial view for the optic nerve. Entropy maps were built from reconstructed vector fields of resolution 2 mm for (a) and 0.2 mm for (b).

3.4 Viewpoint Selection

Viewpoints are finally evaluated based on the information of the 3D entropy map. For a given viewpoint, we compute a 2D projection of the entropy map according to the specific view angle, as illustrated by Figure 4. For each pixel of the 2D projection, we store the minimum entropy value found in the given direction. The projections are hereafter referred to as minimum entropy projection (MEP). The average of the entropy values in the MEP, which we call entropy score, is used as a quality metric for the viewpoint. A viewpoint with a low entropy score is considered to display relevant information about the 3D scene.

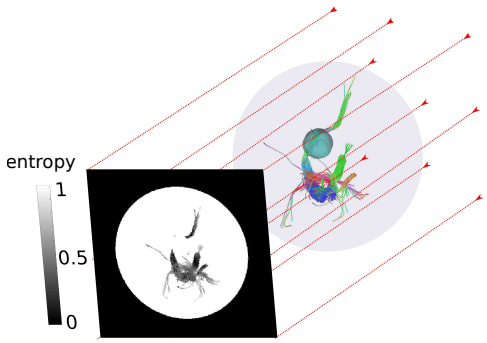

Fig. 4. Minimum entropy projection of a scene with a tumor and several nerves according to a given viewpoint. For clarity, a mesh of the tumor and fibers (colored according to their main direction) is represented instead of the 3D entropy map.

In order to combine the different anatomical structures which compose the scene, the raw entropy map has to undergo some pre-treatments before the projections. First, the entropy map of each cranial nerve is min-max normalized to give the same importance to each nerve in the scene to be visualized. Second, to prevent the occlusion of cranial nerves by themselves, the entropy is computed in a isotropic environment (in terms of number of pixels) to average the entropy on the same number of pixels regardless of the cranial nerve orientation. To do so, a bounding sphere of maximal entropy (entropy=1) centered on the nerves is used.

Finally, the tumor-nerve occlusion is taken into account by including the tumor in the MEPs. A binary segmentation mask of the tumor is produced from the T2-weighted MRI data and registered to dMRI. The tumor voxels are then identified in the entropy map and set to the maximal entropy value (entropy=1). As a result and illustrated in Figure 4, the score of entropy of the MEP where the nerve hides the tumor and vice versa increases and the viewpoint associated is less likely to be selected.

For every scene, the MEPs associated 60 different angles in spherical coordinates (θ, ϕ) with $\theta \in [0, \pi]$ and $\phi \in [-\pi, \pi]$ are produced. A total of 60 view angles, equally distributed over the unit sphere according to [8], are evaluated. MEPs are ranked according to their entropy score. The viewpoints with the lowest and highest entropy scores are considered respectively best and worst viewpoints, as illustrated by Figure 5 in the case of the optic nerve.

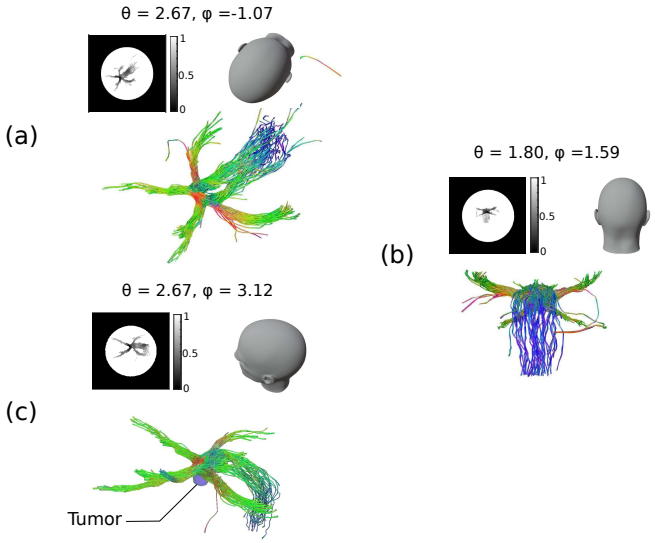

Fig. 5. Result of the best (a) and worst (b) viewpoints selection on the optic nerve. (c) shows the change in best viewpoint if we add a tumor (in purple). For each view, the corresponding MEP is given.

3.5 Validation

A surgical intervention planning context is simulated in order to measure the usefulness of the viewpoint selection algorithm in clinical routine. For all the patients included in our study, the cranial nerves of surgical interest were identified by a neurosurgeon: they correspond to the nerves that are very close to the tumor and might be damaged during surgery. For each patient, the entropy score of 60 viewpoints on the tumor and nerves of surgical interest is computed, as described in Section 3.4. The viewpoints of minimal entropy score $E_{\min}$ and maximal entropy score $E_{\max}$, referred hereafter respectively as best and worst viewpoint, were identified.

The performance of the viewpoint selection is first evaluated qualitatively by comparing the best viewpoint selected to the viewpoint chosen for surgery. The idea is to assess if the selected viewpoint can retrieve or surpass the surgical viewpoint. For this, we asked the neurosurgeon to systematically qualify it as better, equivalent or worse than the surgical viewpoint. In other words, the expert must assess whether the selected view better highlights the nervous structures in relation to the environment (other nerves and tumor) for the purpose of tumor resection.

The global performance of the proposed viewpoint selection method can be quantified from the appreciations given by the expert by computing the prevalence of better or equivalent views such as:

$$\text{prevalence} = \frac{|\text{Sup}| + |\text{Eq}|}{|\text{Sup}| + |\text{Eq}| + |\text{Inf}|}, \tag{3}$$

where Sup, Eq and Inf respectively correspond to the patient cases where the viewpoint associated with E_{min} is superior, equivalent or inferior to the surgical viewpoint according to the expert.

Finally, the entropy scores associated to respectively E_{min} and E_{max} and E_{min} and E_{surg} are compared on the basis of a paired sample t-test. The entropy E_{surg} associated with the surgical viewpoint was estimated from its orientation, which was repositioned in the framework of the 60 viewpoints tested in Section 3.4 and associated with the nearest viewpoint on the basis of a Euclidean distance on the angles.

4 Results

Counting the occurrences of binary score results at the scale of all patients, as explained in Section 3.5 enables us to assess that the viewpoint of best entropy, compared to the surgical viewpoint, provides additional information in 60% of the cases (17/28), a similar level of information in 28% of the cases (7/28) and bring a lower level of information in 14% of the cases (4/28). It was not possible for the neurosurgeon to assess three surgical cases, which is why the occurrence was performed on a total of 28 patients and not 31 as announced in Section 2.2. Overall, the view selection method provides additional or similar information compared to the surgical viewpoint up to 88% (see Equation 3). Regarding the fact that the surgical viewpoint had been carefully selected by the medical expert, this results shows that the entropy score proposed in this work is relevant in a clinical context and meets the requirements of neurosurgeons in terms of visualization.

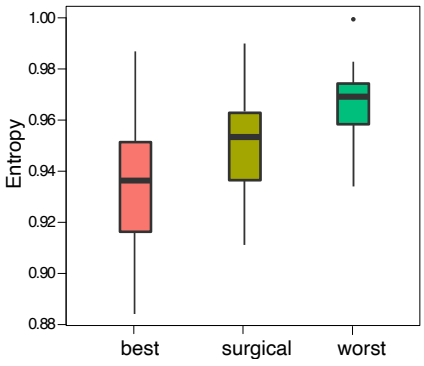

Fig. 6. Distribution of entropy associated with viewpoints in patients. The viewpoints associated to E_{min}, E_{max} and the surgery are respectively annotated "best", "worst" and "surgical".

Moreover, a statistical analysis of the entropy scores associated with the best, surgical and worst viewpoint was conducted as proposed in Section 3.5. The Figure 6, illustrates the distribution of the entropy scores $E_{\min}$, E_{surg} and $E_{\max}$ for all the patients. A paired sample t-tests shows a significant difference between the entropy scores of the best and the worst viewpoints (p-value = 3e-13) and between the entropy scores of the best and surgical viewpoints (p-value = 2e-06). The best viewpoints scores significantly better than the surgical viewpoint, which indicates that the surgical viewpoint selection can be improved by our algorithm.

Furthermore, as illustrated on Figure 7, the best viewpoint selected with our algorithm clearly depicts the tumor and the displaced nerves. Although occlusion areas still exist, this viewpoint seems to provide the best trade-off between showing the nerves of interest in their entirety and minimizing occlusion with the tumor and the most disorganized fibers. Figure 7 shows the cases of three patients with respectively medium, high and low information gains from the surgical viewpoint as depicted by the curves on top of each row.

In the case of patient 1, the worst viewpoint is particularly unfavorable : high entropy fibers are present in the foreground, causing occlusion of both the tumor and the nerves. On the contrary, from the best viewpoint, the trajectory of the nerves V, III, and NF can be clearly observed, even if the nerve III and the tumor partially overlaps. The surgical viewpoint gives less information on the nerves and their context because the tumor masks nerves III and V and NF is hidden behind III, but still outperforms the worst view. The case of patient 2 is the most interesting as regards the contribution of our algorithm. Because of the important size of the tumor and the very close location of the nerves, very few viewpoint enables an optimal representation of the scene. Few choices were offered for the approach way of the tumor, resulting in a very poor visualization on the surgical viewpoint where the huge tumor masks almost completely the nerves NF and V. Even for this difficult case, our algorithm was able to find a viewpoint where all the nerve and their trajectory can be clearly identified. This representation can therefore be seen by the surgeon before the operation and used for the pre-surgery planning. In the case of patient 3, where the gain is low, the best and surgical viewpoint offers a very similar information on the nerve trajectory and tumor position. In comparison, the worst viewpoint appear very poor: the tumor and nerve NF are almost completely hidden by the most disorganized fibers of the nerve V, making the scene very difficult to understand. In all the illustrated cases, the entropy score seems to match correctly the qualitative evaluation of the different viewpoints.

5 Conclusion

In this paper, we presented a viewpoint selection framework for fibrous structures applied in the context of tumors surrounded by cranial nerves. The entropy of the direction of the white matter fibers was identified as an interesting metric to enhance the areas of the scene with high informative content (i.e. inside a nerve),

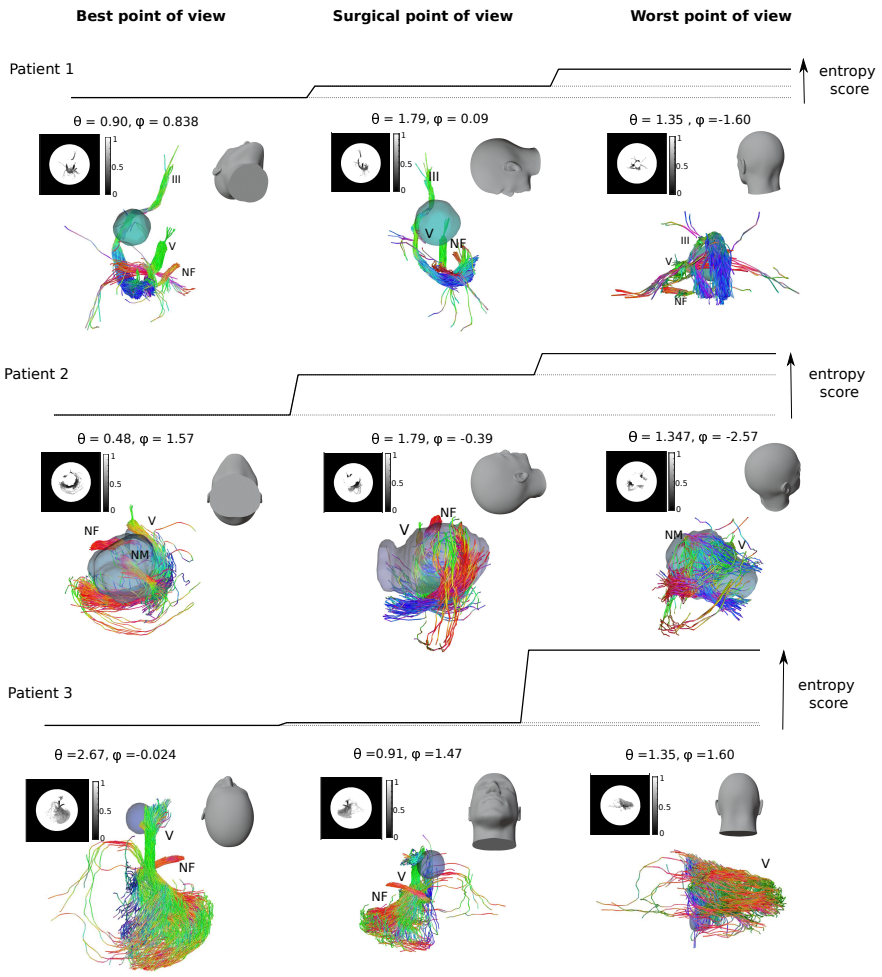

Fig. 7. MEPs, anatomical reference and scene visualization for the surgical viewpoint and the best and worst viewpoints returned by our algorithm. The difference of entropy score between the 3 viewpoints is given through a step function. A partial transparency of the tumor helps the visualization of the fibers inside and behind it.

in accordance with the concerns of the surgery. The occlusion caused by the tumor was taken into account. The best viewpoints selected by our algorithm were judged equivalent or superior than the viewpoint used for surgery in 88% of the cases. The difference of quality score for those two viewpoints is significant. This results indicates that neurosurgeons could benefit from the present algorithm in the choice of the surgery viewpoint. However, we acknowledge some limitation to this work; in clinical routine, the choice of the surgical viewpoint is restricted by anatomical considerations. Some viewpoints can not be realistically chosen,

for instance viewpoints going through the face or the neck of the patient. As a future work, we want to include such anatomical constraints in the viewpoint selection process. We also plan to extend the use of the entropy metric to filter tractography fibers for an enhanced visualization.

References

1. Bonaventura, X., Feixas, M., Sbert, M., Chuang, L., Wallraven, C.: A survey of viewpoint selection methods for polygonal models. Entropy **20**(5), 370 (2018)
2. Borkar, S.A., Garg, A., Mankotia, D.S., Joseph, S.L., Suri, A., Kumar, R., Kale, S.S., Sharma, B.S., et al.: Prediction of facial nerve position in large vestibular schwannomas using diffusion tensor imaging tractography and its intraoperative correlation. Neurology India **64**(5), 965 (2016)
3. Chan, M.Y., Qu, H., Wu, Y., Zhou, H.: Viewpoint selection for angiographic volume. In: International Symposium on Visual Computing. pp. 528–537. Springer (2006)
4. Chen, M., Feixas, M., Viola, I., Bardera, A., Shen, H.W., Sbert, M.: Information theory tools for visualization. CRC Press (2016)
5. Jacquesson, T., Cotton, F., Attyé, A., Zaouche, S., Tringali, S., Bosc, J., Robinson, P., Jouanneau, E., Frindel, C.: Probabilistic tractography to predict the position of cranial nerves displaced by skull base tumors: Value for surgical strategy through a case series of 62 patients. Neurosurgery (2018)
6. Jacquesson, T., Frindel, C., Kocevar, G., Berhouma, M., Jouanneau, E., Attyé, A., Cotton, F.: Overcoming challenges of cranial nerve tractography: a targeted review. Neurosurgery **84**(2), 313–325 (2018)
7. Joo, W., Yoshioka, F., Funaki, T., Rhoton, A.L.: Microsurgical anatomy of the trigeminal nerve. Clinical Anatomy **27**, 61–88 (2014). https://doi.org/10.1002/ca.22330
8. Leopardi, P.: A partition of the unit sphere into regions of equal area and small diameter. Electronic Transactions on Numerical Analysis pp. 309–327 (March 2006)
9. Mühler, K., Neugebauer, M., Tietjen, C., Preim, B.: Viewpoint selection for intervention planning. In: EuroVis. pp. 267–274 (2007)
10. Rhoton, A.L.: Microsurgical anatomy of the posterior fossa cranial nerves. Clinical Neurosurgery **26**, 398–462 (1979)
11. Samii, M., Gerganov, V.M.: Petroclival meningiomas: quo vadis? World neurosurgery **75**(3-4), 424 (2011)
12. Smith, S.M., Jenkinson, M., Woolrich, M.W., Beckmann, C.F., Behrens, T.E., Johansen-Berg, H., Bannister, P.R., De Luca, M., Drobnjak, I., Flitney, D.E., et al.: Advances in functional and structural mr image analysis and implementation as fsl. Neuroimage **23**, S208–S219 (2004)
13. Song, F., Hou, Y., Sun, G., Chen, X., Xu, B., Huang, J.H., Zhang, J.: In vivo visualization of the facial nerve in patients with acoustic neuroma using diffusion tensor imaging–based fiber tracking. Journal of neurosurgery **125**(4), 787–794 (2016)
14. Tournier, J.D., Smith, R., Raffelt, D., Tabbara, R., Dhollander, T., Pietsch, M., Christiaens, D., Jeurissen, B., Yeh, C.H., Connelly, A.: MRtrix3: A fast, flexible and open software framework for medical image processing and visualisation. NeuroImage p. 116137 (2019)
15. Xu, C., Prince, J.L.: Snakes, shapes, and gradient vector flow. IEEE Transations on Image Processing (March 1998)

16. Yoshino, M., Abhinav, K., Yeh, F.C., Panesar, S., Fernandes, D., Pathak, S., Gardner, P.A., Fernandez-Miranda, J.C.: Visualization of cranial nerves using high-definition fiber tractography. Neurosurgery **79**, 146–165 (2016). https://doi.org/10.1227/NEU.0000000000001241